

Article

Custom-Designed Pre-Chamber: Investigating the Effects on Small SI Engine in Active and Passive Modes

Paolo Sementa , Cinzia Tornatore * , Francesco Catapano, Silvana Di Iorio  and Bianca Maria Vaglieco 

Institute of Science and Technology for Sustainable Energy and Mobility, CNR (Italian National Research Council), Via Marconi 4, 80125 Napoli, Italy; paolo.sementa@stems.cnr.it (P.S.); francesco.catapano@stems.cnr.it (F.C.); silvana.diiorio@stems.cnr.it (S.D.I.); biancamaria.vaglieco@stems.cnr.it (B.M.V.)

* Correspondence: cinzia.tornatore@stems.cnr.it

Abstract: This work shows the results of an experimental campaign carried out in two spark ignition engines, a small optical research engine and its commercial counterpart, using a turbulent ignition system (pre-chamber) specifically designed for small engines. Advanced optical techniques and conventional methods were used to study the combustion process under various operating conditions. The pre-chamber operated actively in the research engine and passively in the commercial engine. Results showed that the pre-chamber configuration resulted in an increase in indicated mean effective pressure (IMEP) and a decrease in the coefficient of variation (CoV) of IMEP. These improvements compensated for challenges such as slow methane combustion rate, poor lean burn capability, and air displacement. In addition, the pre-chamber configuration exhibited lower fuel consumption and specific exhaust emissions compared to the standard ignition system. The novelty of this work lies in the successful implementation of the turbulent ignition system as a retrofit solution for SI engines, showing improved combustion efficiency and lower emissions. The study goes beyond previous efforts by demonstrating the benefits of the pre-chamber configuration in small engines without requiring extensive modifications. The results provide valuable insights into the automotive industry's pursuit of engine optimization and highlight the significance of innovative approaches for spark ignition engines in contributing to sustainable mobility.

Keywords: pre-chamber design; SI engine; active pre-chamber; passive pre-chamber; optical engine



Citation: Sementa, P.; Tornatore, C.; Catapano, F.; Di Iorio, S.; Vaglieco, B.M. Custom-Designed Pre-Chamber: Investigating the Effects on Small SI Engine in Active and Passive Modes. *Energies* **2023**, *16*, 5097. <https://doi.org/10.3390/en16135097>

Academic Editor: Theodoros Zannis

Received: 29 May 2023

Revised: 28 June 2023

Accepted: 28 June 2023

Published: 1 July 2023



Copyright: © 2023 by the authors. Licensee MDPI, Basel, Switzerland. This article is an open access article distributed under the terms and conditions of the Creative Commons Attribution (CC BY) license (<https://creativecommons.org/licenses/by/4.0/>).

1. Introduction

Increasing concerns about fuel shortages and environmental issues have led to extensive research into new technologies for internal combustion engines to reduce fuel consumption and lower CO₂ and pollutant emissions while improving performance.

Recently, modern spark ignition engines have undergone a transition towards the adoption of direct injection systems, known as gasoline direct injection (GDI). This shift is driven by the desire to enhance engine efficiency and attain higher performance [1,2]. Direct injection of fuel into the combustion chamber brings several advantages, including improved knock resistance and higher volumetric efficiency. For liquid fuels, this is primarily due to improved air cooling as a result of fuel evaporation. In the case of gaseous fuels, direct injection provides better cylinder filling by displacing a portion of the air that enters the cylinder when operating in port-fuel mode [3,4]. Consequently, this substitution of air for gaseous fuel helps to reduce the limits of achievable specific power. In addition, the higher pressure and improved precision of the GDI injectors allow more precise control of the fuel quantity, resulting in improved efficiency, especially in the part-load conditions and in dynamic operation. It should be noted, however, that the direct injection system is comparatively more complex and comes with a higher cost when compared with its counterpart, intake manifold injection.

One of the proposed solutions to significantly improve the efficiency of SI engines is the use of lean mixtures, which can reduce unburned hydrocarbon and CO₂ emissions,

especially during cold start [5–7]. The introduction of lean mixtures into the combustion chamber leads to a decrease in flame speed and, thus, to a lower rate of heat release. Moreover, the application of lean stratified combustion can potentially lead to engine stability issues, especially with respect to cycle-to-cycle variation (CCV). The slowdown in flame speed associated with lean stratified combustion can contribute to CCV, which has a significant impact on engine emissions and performance. Instabilities during engine operation, including vibration and noise, can affect power output. Conversely, reducing CCV can increase power output while maintaining fuel economy, thereby increasing overall efficiency.

CCV in SI engines can be influenced by multiple factors, such as turbulence intensity in the combustion chamber, air/fuel ratio, presence of residual or recirculated exhaust gasses in the cylinder, spatial non-uniformity of mixture composition near the spark plug, spark characteristics (including energy and duration), and flame core development. In general, an increase in the burning rate and an improvement in flame front propagation lead to an increase in engine stability [8], and this can be achieved in several ways, especially under lean conditions. New combustion strategies, such as partial fuel stratification, have demonstrated effectiveness in stabilizing lean combustion in direct injection spark ignition engines [9]. Despite the benefits of GDI technology, it also presents certain drawbacks, including an increase in exhaust emissions such as hydrocarbons (HC), carbon monoxide (CO), and particulate matter. This is primarily due to the short duration available for fuel vaporization and mixture formation to achieve charge stratification for overall lean combustion. Furthermore, the impingement of fuel on the piston head and cylinder wall contributes to these exhaust emissions [10–13].

New architectures, such as optimized pre-chambers, allow the flame speed and turbulence to be increased [14,15]. A pre-chamber consists of a very small auxiliary chamber connected to the main combustion chamber designed to initiate a flame front that rapidly ignites the air-fuel mixture in the main chamber.

The mixture in a pre-chamber can be realized either by scavenging the mixture from the main chamber during the compression stroke (passive pre-chamber) or by an additional external fuel supply (active pre-chamber). The pre-chamber allows both stratified charge combustion and very lean mixture combustion, which can reduce fuel consumption as in direct injection engines [16] without greatly increasing pollutant emissions.

In both passive and active configurations, during the compression stroke, the pre-chamber is filled with the intake charge present in the main combustion chamber. As the piston approaches the top of the compression stroke, the spark plug ignites the air-fuel mixture in the pre-chamber, causing a high-energy jet of flame and hot gasses to be expelled through small holes into the main combustion chamber. The pre-chamber acts as a dedicated ignition source for the leaner mixture in the main chamber, providing faster and more consistent combustion initiation. In the active pre-chamber configuration, a small amount of fuel is injected during the compression stroke, enriching the fuel-air mixture around the spark plug [17], further increasing the stability and reliability of the ignition and combustion processes in the main chamber. Active pre-chambers can be supplied with either liquid or gaseous fuels, which brings some advantages in mixture formation. There are examples of fuel supply to an active pre-chamber using fuel vapor [18], a premixed fuel-air mixture [19], and methane or hydrogen [20].

The improvement in combustion stability and fuel efficiency through pre-chambers is highly dependent on an appropriate geometric design that allows proper pre-chamber filling and jet ejection, ultimately leading to efficient main chamber ignition. Optimization of the pre-chamber design takes into account aspects such as pre-chamber volume, internal shape, nozzle orifice layout and diameter, swirl control, injector location, spark plug arrangement, and turbulence generation. To fine-tune these design parameters for optimal performance and efficiency, the scientific community uses computational fluid dynamics simulations (CFD) [21] and experimental studies. From an experimental point of view, several researchers have studied the influence of different geometric parameters

on the combustion process in metal engines [22]. In addition, optical studies using optical techniques such as natural flame luminosity imaging, OH* chemiluminescence, infrared emission, and planar laser-induced fluorescence (PLIF) have played a complementary role by characterizing jet ejection and providing valuable insight into ignition within the engine main chamber [23,24]. The effects of nozzle diameter on an active pre-chamber jet and engine performance were investigated, and it was found that a pre-chamber with multiple holes and a small hole diameter can improve thermal efficiency, but excessively small hole diameters can lead to flame quenching and misfire [25,26]. With regard to spark plug design, spark plug type, direction, position, and electrode spacing of the spark plug have a significant effect on flame core development and combustion [27].

Properly designed pre-chambers can significantly extend engine lean-burn limit of the engine and increase efficiency [28], but one of the disadvantages of integrating a pre-chamber into an engine head is the associated cost. Installation of a pre-chamber requires modification of the cylinder head, which may necessitate a redesign of coolant passages or other features.

This paper reports on the design and testing of a prototype pre-chamber intended as a retrofit for small commercial engines without the need to modify the cylinder head and engine components. The pre-chamber was designed using the virtual design program SolidWorks CAD. The main design goal was to include in the original engine head, particularly in the spark plug location, the pre-chamber endowed with both a commercial spark plug and injector. Once designed and manufactured, the pre-chamber was able to be installed in a single-cylinder optical engine and in a commercial engine, being used in both active and passive modes. Its effects on the combustion process, engine performance, and emissions were studied.

The first part of the experiments was conducted in an optically accessible small spark ignition engine running on methane and gasoline, and the pre-chamber was operated in active mode. First, methane was injected into the pre-chamber and gasoline into the intake manifold at an engine speed of 2000 rpm; subsequently, methane was injected into both the pre-chamber and the intake manifold at 2000 rpm and 4000 rpm. At both engine speeds, the optical engine ran with the throttle wide open (WOT) and in stoichiometric and lean mode. The engine was alternately equipped with the standard spark plug and with the pre-chamber, which was equipped with a direct fuel injector and a spark plug. The combustion process was characterized by the acquisition of the indicated data for thermodynamic analysis and the application of optical techniques, which provide a powerful tool for the detailed description of the combustion process with a high spatial and temporal resolution allowing a local analysis of the fundamental processes.

The second part of the experimental activity was carried out in a commercial small spark ignition engine with the same characteristics as the research engine, running on gasoline and with the pre-chamber operating in passive mode. This further experimental campaign is intended to demonstrate the capability of the designed pre-chamber system to be installed in the commercial engine head with no modifications and to give good results in terms of engine performance improvements and also in its simpler configuration, i.e., without additional injector (passive mode). The experiments were performed at engine speeds of 2000, 3000, 4000, and 5000 rpm in stoichiometric and lean modes. The engine was alternately equipped with the standard spark plug and with the pre-chamber operating in passive mode. In order to obtain the same cylinder peak pressure in motored conditions in the two configurations, a WOT condition was used for the pre-chamber, and for the standard ignition configuration, the tests were performed at partial load (PL). The combustion process was characterized by collecting the indicated data for thermodynamic analysis, and exhaust emissions were measured under all engine operating conditions.

This paper is intended to represent an important advance in knowledge in this field: This paper describes the pre-chamber design compatible with a commercial small displacement engine and the effects of pre-chamber ignition compared to the original spark system on the combustion process under stoichiometric and lean-burn operating conditions. The

optical investigation in the research engine provides important information about the ignition mechanism and combustion evolution, which results from the use of the pre-chamber through high spatial and temporal visualization under real engine-like conditions. On the other hand, the tests carried out on the commercial engine support the conclusions on the efficiency improvements possible by using the pre-chamber, especially for lean mixtures.

2. Experimental Apparatus

2.1. Pre-Chamber

The pre-chamber was designed to fit inside the engine head, which is identical to the commercial engine and the optically accessible research engine. It was designed to be housed in the spark plug hole: the main challenge was to fit all the new components into an existing, very small geometry designed only for the spark plug. Figure 1 shows the complete ignition system in conjunction with the SI engine head, the pre-chamber, and a detail of the pre-chamber tip with the holes.

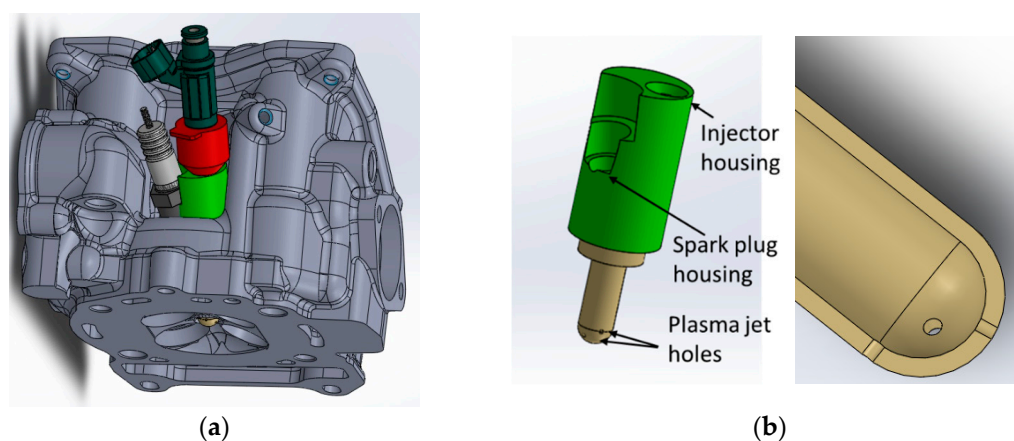


Figure 1. Pre-chamber mounted in engine head (a), detail of pre-chamber (b). The housing for the spark plug and the injection nozzle is shown in green, and the combustion pre-chamber is in gray.

The new ignition system consists of five different parts:

- Combustion pre-chamber (golden part): The mixture of air and fuel is generated in this component. The mixture ignites thanks to the spark plug, and due to the resulting increase in temperature and, thus, pressure, the mixture passes through the holes into the combustion chamber at a very high speed. The main objectives in the development of this component were: Minimizing the volume to minimize the impact on the compression ratio. Optimizing the shape, number, and orientation of the holes to maximize the propagation speed of the plasma jet and, thus, the flame in the combustion chamber.
- Spark plug and injector housing (green part): The hole that originally contained the spark plug has a maximum diameter of 24 mm. Due to the limited volume, the spark plug and the injector could not be inserted in parallel. After a careful analysis focused on reducing dead volume and possible losses, it was decided to insert the injector along an axis parallel to the original spark plug hole and the spark plug at an angle of 14° to the axis of the injector. In this way, it was possible to accommodate the two components while facilitating assembly and disassembly operations.
- Spark plug: an NGK-ER8EH-N spark plug was chosen for the pre-chamber for its small size (thread diameter of 8 mm, hexagon of 13 mm, and thread length of 19 mm).
- Injector: A commercially available “Synerject Strata” injector was selected, designed to inject an air-gasoline mixture in a direct injection system for gasoline engines. The injector was modified to inject gaseous fuel: It was coupled with an adapter that has the external geometry of the commercial GDI injector. On the inside, the adapter is

equipped with an appropriately sized channel that allows methane to be injected into the pre-chamber, optimizing mixture formation.

- Injector adapter (red part): An injector extension/adapter was designed to allow fuel to be injected into the pre-chamber. The geometry of the adapter was designed based on that of the injector. One end of the extension faces the combustion chamber, and the other is connected to the injector, which in turn is connected to a rail. In the case of the passive pre-chamber, there is no injector (dark green part), and the injector adapter is used only as a cap.

Different pre-chambers with different numbers of holes and diameters were designed and tested [29]. In this article, the results with four holes with a diameter of 1 mm are described.

Figure 2 shows a section of the engine head with the pre-chamber and a picture showing the pre-chamber at the spark plug location of the engine. In the scientific literature, it was found that if the volume of the pre-chamber exceeds 2.4% of the dead volume, the disadvantages of reducing the compression ratio could exceed its advantages [30]. In this study, the pre-chamber was not optimized for performance; it has a volume of 2.2 cm³, which corresponds to 7.2% of the dead volume and results in a reduction of the compression ratio from 9:1 to 8.5:1. Nevertheless, the performances of the engine equipped with the pre-chamber are similar and, in certain conditions, even higher than those obtained with the standard ignition system.

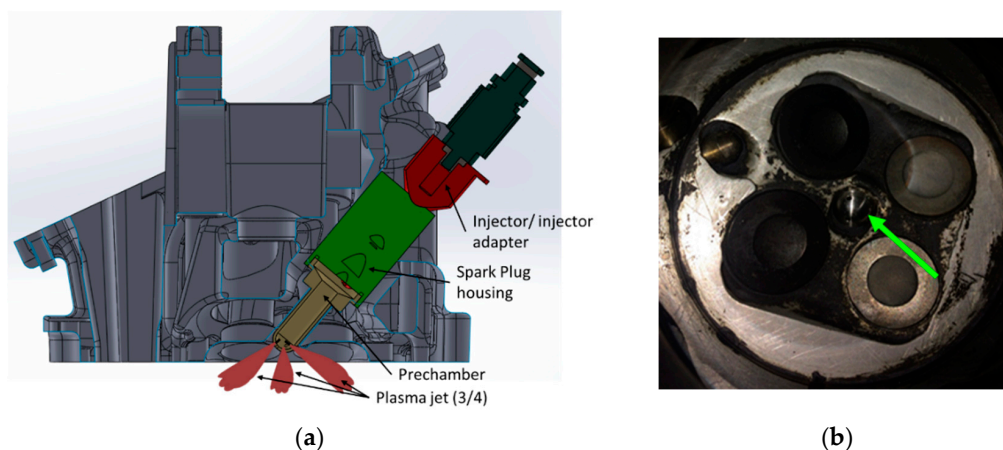


Figure 2. Section through the engine head with the pre-chamber (a), pre-chamber tip in the center of the head (green arrow) (b).

2.2. Engines Setup and Procedures

The new ignition system (pre-chamber) was tested on two small single-cylinder engines of 250 cm³ SI with the same head. The difference between the engines is that one is the commercial version, and the other has been modified to be widely optically accessible. The commercial engine has a maximum power of 16 kW at 8000 rpm and a maximum torque of 20 Nm at 5500 rpm. In the optical version, the speed is limited to 5000 rpm, so the maximum power is 7.9 kW, and the maximum torque is 14.7 Nm (measured at 5000 rpm). The head features a four-valve, pent-roof geometry chamber with a centered spark plug. The bore and stroke of the engines are 72 mm and 60 mm, respectively, and the geometric compression ratio is 9:1 with the standard ignition system; as previously reported, when the pre-chamber is fitted, the compression ratio drops to 8.5:1 due to the higher dead volume. In both engines, the main injection is in the intake manifold (port fuel injection, PFI), and methane is supplied to the engine from a pressurized bottle with a pressure regulator set at 8 bar. The fuel line is split into two rails to supply both the port injector and the pre-chamber.

The in-cylinder pressure is measured by a quartz pressure transducer mounted flush in the area between the intake and exhaust valves. The in-cylinder pressure, rate of chemical energy release, and associated parameters are evaluated for each cycle and/or averaged

over 500 consecutive cycles [7]. A lambda sensor is installed on the engine exhaust to measure the air/fuel ratio. Injection timing is controlled by the ETU (Engine Timing Unit) multi-channel system, as is ignition timing. Only in the commercial engine were HC, CO, and CO₂ emissions measured using an NDIR analyzer, and NO_x emissions were measured using chemical sensors.

The standard spark plug and pre-chamber are mounted alternately on the engines. The duration of the coil charge is set to 4 ms in both cases so as not to change the energy delivered by the spark to the air-fuel mixture. Details of the engines' characteristics are shown in Table 1.

Table 1. Specifications of the SI single cylinder four stroke engines.

Parameter	Value
Displacement [cm ³]	250
Bore [mm]	72
Stroke [mm]	60
Connecting road [mm]	130
Compression ratio	9:1
Valve timing [°CA]	Intake Valve: Opening @ 6 After Top Dead Center and Closing @ 50 After Bottom Dead Center, Exhaust Valve: Opening @ 4 Before Bottom Dead Center and Closing @ 1 After Top Dead Center

In the optically accessible engine, a wide section of the concentric flat-bottomed piston bowl is replaced by a sapphire window. An elongated piston arrangement is used, equipped with two self-lubricating piston rings to prevent the lubricating oil from getting on the window during engine operation. The upper ring, near the top of the piston, is made of a high carbon/Teflon bronze composite to better withstand the high temperatures of combustion. The lower piston ring, protected from temperature by the upper ring, is made of Teflon-Bronze to provide a better seal. Moreover, for the lower part of the transparent single-cylinder engine, a special lubricating oil and coolant conditioning unit is used; it contains a pump for oil and another for water. The oil pressure in the circuit is adjusted by a pressure control valve (overflow valve). The water circuit is equipped with a coolant/water heat exchanger and a coolant heater. The heat exchanger is used to cool the water during engine operation and the engine-lubricating oil via the coolant/oil heat exchanger. The coolant heater is instead designed to heat the coolant and lubricating oil during engine warm-up to stabilize the engine operating condition before starting the experiments, as the duration of the optical engine tests is insufficient to stabilize temperatures.

Figure 3 shows a detail of the optical engine and experimental setup for cycle-resolved 2D imaging of natural luminosity. A 45° tilted UV-visible mirror, located at the bottom of the optical section of the engine, reflects the light emitted during the combustion process that has passed the transparent piston. In this way, the light is reflected toward the optical detection unit, which differs depending on the optical technique applied.

For cycle-resolved flame visualization, images were acquired using a fast 16-bit 1024 × 1024 pixel CMOS (complementary metal-oxide semiconductor) camera coupled with a Nikon lens with a 105 mm focal length and f/3.8. The optical configuration provided a spatial resolution of 100 μm/pixel. A camera region of interest of 512 × 512 pixels was selected, and a frame rate of 12,500 frames per second, corresponding to an exposure time of 80 μs, was set to achieve the best match between spatial and temporal resolution, considering the low luminosity of methane combustion compared to gasoline. The spectral wavelength range of the camera is 380–700 nm.

UV-visible digital imaging of the combustion process was carried out using an ICCD (Intensified Charge Coupled Device) camera, PIMAX 3—Princeton Instruments, with a Nikon f/3.8 UV lens with a focal length of 78 mm. In the case of engine operation at 2000 rpm, using the traditional ignition system, an image is acquired every 2° Crank Angle—°CA (166.6 μs), with an exposure time of 2 °CA (166.6 μs). With the use of the

pre-chamber, an image is acquired every $^{\circ}\text{CA}$, corresponding to $83.3\ \mu\text{s}$ with an exposure time of $1\ ^{\circ}\text{CA}$.

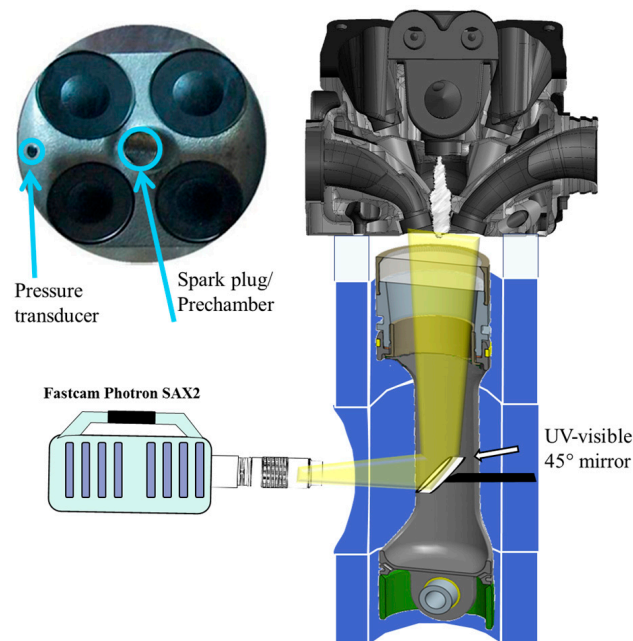


Figure 3. Experimental apparatus: optical engine and optical setup for investigations in the combustion chamber.

The first time of acquisition also varies depending on the ignition system used. In the case of a traditional ignition system, the start corresponds to the spark timing (ST); using the pre-chamber, the acquisition starts after the ST because the combustion inside the pre-chamber takes about $10\ ^{\circ}\text{CA}$ (@2000 rpm) to propagate through the orifices.

During each test, 20 frames are acquired, corresponding to $40\ ^{\circ}\text{CA}$ with the traditional ignition system and to $20\ ^{\circ}\text{CA}$ in the case of pre-chamber. To obtain a more accurate estimation of the combustion process, for each of the 20 frames, the camera acquires five images corresponding to five different cycles to allow calculating an average image.

A bandpass filter (centered at 310 nm) was coupled to the ICCD camera to measure the two-dimensional, spatially resolved chemiluminescence of the OH^* radical.

The synchronization between the engine crankshaft, the in-cylinder process, and the optical measurements was obtained through the AVL Crank Angle Encoder signal and the AVL ETU, used to generate the trigger signals for the injectors (both in the pre-chamber and in the intake manifold) and the ignition coil. In this way, through two signals generated by the Encoder, Trigger, and CDM, it was possible to determine the crank angles where the optical data were acquired. Moreover, during the optical measurements, in-cylinder pressure, pressure, and temperature of the intake air and the lambda value were acquired and recorded on the AVL Indimodul, using TTL signals together with the signal acquired through the crank angle encoder.

The detected images were post-processed using the open software ImageJ, which allows geometric information such as the flame area and radius to be obtained from the brightness of each average image. The procedure used is shown in Figure 4 and is characterized by the basic steps described in a previous article [7]. Prior to the acquisition of all sequences, the background was detected in motored condition. Then, each 16-bit grayscale image was treated by subtracting the background (original image background). Then, the intensity and contrast of the images were optimized to obtain an image that is much sharper and brighter than the original (treated image). Then, a threshold was set, and the image was binarized (binarized image). The non-zero pixels of the binarized image were counted to obtain the flame area (in pixels). For both the standard ignition and for

pre-chamber case, starting from the total flame, which was obtained by summing all flame areas in the image, the flame radius was calculated as the radius of the equivalent flame circumference. The corresponding flame speed was calculated from the flame radius.

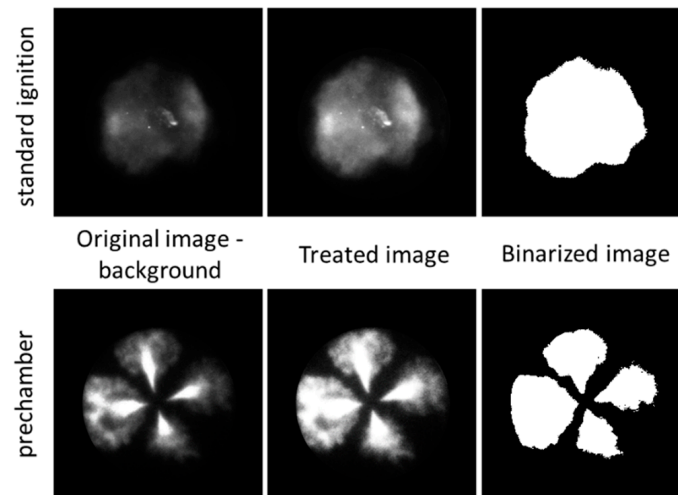


Figure 4. Procedure for image processing.

The fuels used in these activities were methane and European commercial gasoline. The chemical and physical properties are listed in Table 2.

Table 2. Fuel properties.

Fuel Property	Gasoline	Methane
Formula	C4–C12	CH ₄
Molecular weight [kg/kg mol]	100–105	16.04
Carbon [mass %]	85–88	75
Hydrogen [mass %]	12–15	25
Oxygen [mass %]	2.7	-
Density [kg/m ³]	720–775	0.67
Boiling point [°C]	27–225	−161.4
Vapor pressure [kPa at 38 °C]	48–103	-
Specific heat [kJ/kg K]	2	2.22
Viscosity [mPa·s at 20 °C]	0.37–0.44	0.011
Lower Heating Value [MJ/kg]	42–44	50
Auto ignition temperature [°C]	257	600
Research Octane Number	98	>120
Flammability limit [vol %]	1.4/7.6	5.3/14
Stoichiometric air/fuel	14.7	17.24

3. Results and Discussion

The “results and discussion” section is divided into two parts: in the first part, the effect of the pre-chamber (active mode) on the combustion phenomenon in the optical research engine using high-speed imaging, UV visible imaging, and OH* chemiluminescence. In the second part of the section, the pre-chamber (in passive mode) was used in the commercial SI engine to evaluate how it affects engine performance and emissions.

In the optical engine, the active configuration was chosen to induce the phenomena taking place in the pre-chamber in a more controlled way. In the commercial version of the engine, the passive pre-chamber was used because it is more realistic and useful in terms of retrofit, as it would be simpler and cheaper without an additional injection system.

3.1. Pre-Chamber in the Optical Research Engine

3.1.1. Engine Operating Conditions in the Optical SI Research Engine

All experiments were performed at WOT; the intake air temperature was set to 298 K, and the cooling water temperature to 333 K. Two different injection systems were chosen for the optical SI engine: (1) methane injection at 8 bar in both the pre-chamber and the intake manifold; (2) methane injection at 8 bar in the pre-chamber and gasoline in the intake manifold.

Twelve conditions were tested at 2000 and 4000 rpm, characterized by different equivalence ratios: $\lambda = 1.00$, $\lambda = 1.15$, $\lambda = 1.30$, $\lambda = 1.60$, with the standard ignition system (SIS) and with the pre-chamber ignition system (PC).

Finally, in order to optimize exhaust emissions with respect to HC, the end of fuel injection in the pre-chamber was set at 190 °CA BTDC (firing TDC).

The details of the engine performance at the selected operating conditions are given in Table 3 in terms of IMEP and CoV of IMEP. The values of CoV of IMEP were similar to those of the commercial reference engine (see next section), but the IMEP is lower due to the lower compression ratio of the optically accessible engine (9:1 versus 11.5:1).

Table 3. Details of the selected engine operating conditions.

Fuel PFI	Ignition System	Speed [rpm]	λ	DOI (PFI) [°CA]	DOI (PC) [°CA]	IMEP [bar]	CoV _{IMEP} [%]	ST [°CA BTDC]	Test #
Gasoline	SIS	2000	1.00	125		5.2	0.9	25	1
	SIS	2000	1.15	115		4.9	1.4	25	2
	PC (CH ₄)	2000	1.00	120	10	4.5	2.8	20	3
	PC (CH ₄)	2000	1.15	112	10	4.4	4.3	22	4
	PC (CH ₄)	2000	1.30	105	10	4.0	2.7	25	5
	PC (CH ₄)	2000	1.60	88	10	3.7	4.7	33	6
CH ₄	SIS	2000	1.00	115		5.3	2.9	24	7
	SIS	2000	1.30	100		4.6	7.4	24	8
	PC (CH ₄)	2000	1.00	110	10	5.1	2.0	20	9
	PC (CH ₄)	2000	1.30	90	10	4.2	2.9	20	10
	SIS	4000	1.00	230		5.9	3.8	30	11
	SIS	4000	1.30	190		3.4	2.5	30	12
	PC (CH ₄)	4000	1.00	220	10	5.8	1.9	38	13
	PC (CH ₄) (CH ₄)	4000	1.30	180	10	5.0	2.7	38	14

3.1.2. Indicated Data Analysis

Figures 5 and 6 show the comparison between in-cylinder pressure and Rate of Heat Release (ROHR) averaged over 500 consecutive cycles for the turbulent ignition (pre-chamber) system and the standard ignition configuration at 2000 and 4000 rpm—WOT in stoichiometric and lean modes. The ROHR curves are obtained from the in-cylinder pressure signal using the first law of thermodynamics. The blue curves are the indicated data for the standard ignition configuration, and the green curves represent the indicated data when the pre-chamber is used.

Figure 5 refers to tests #1–#2, where gasoline is port injected, and to tests #3–#6, where methane is injected into the pre-chamber and gasoline is injected in PFI mode at 2000 rpm. Figure 6 refers to tests #7–#8, 11–#12, where the methane is port injected, and to tests #9–#10, #13–#14, where the methane is injected into both the intake manifold and the pre-chamber, at 2000 rpm (a) and 4000 rpm (b).

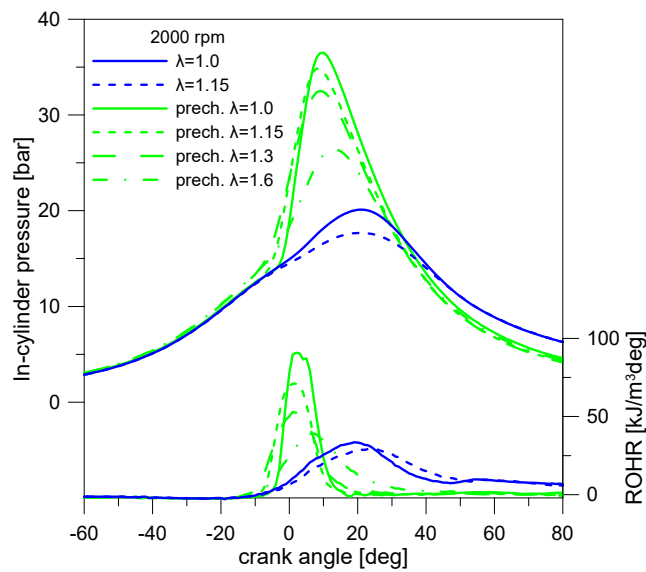


Figure 5. In-cylinder pressure and ROHR curves for pre-chamber and standard ignition system under stoichiometric and lean conditions at 2000 rpm with gasoline port injection (tests #1 to #6).

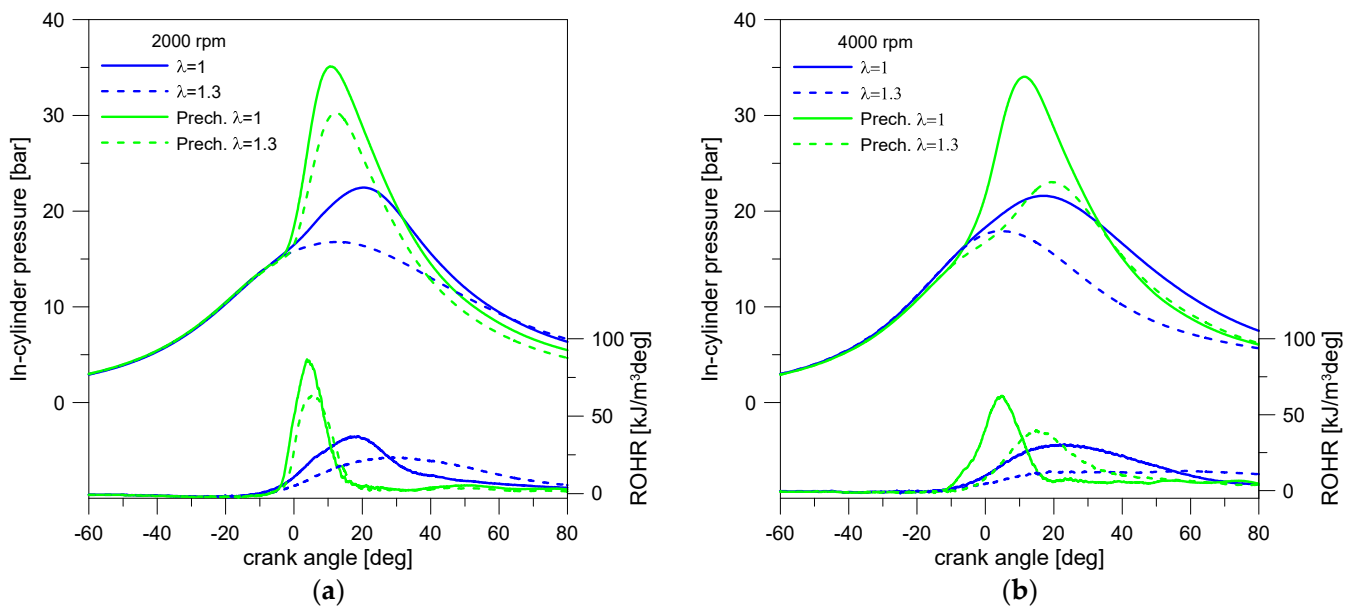


Figure 6. In-cylinder pressure and ROHR curves for pre-chamber and standard ignition system (a) under stoichiometric and lean conditions at 2000 rpm (tests #7 to #10), (b) under stoichiometric and lean conditions at 4000 rpm (tests #11 to #14) with methane port injection.

For all conditions shown in Figures 5 and 6, the in-cylinder pressure and ROHR curves increase sharply during pre-chamber combustion, indicating faster combustion compared to the conventional spark plug. The curves in the pre-chamber ignition mode are very narrow compared to the standard configuration, indicating a shorter combustion duration. Under all conditions, both stoichiometric and lean combustion, the pre-chamber configuration exhibits higher cylinder pressure than the standard spark plug configuration, despite the lower compression ratio. The increase in pressure can be attributed to a sharp reduction in combustion duration and a resulting better combustion phasing as well as lower thermal losses. The overall combustion efficiency is improved by the turbulence generated by the pre-chamber within the main combustion chamber and the faster propagation of the flame front obtained with the plasma jets outgoing from the pre-chamber.

For lean mixtures, the combustion is slower and more retarded than in the stoichiometric case, as highlighted by the ROHR curves. This is due to the lower flame speed of lean mixtures. On the other side, using the pre-chamber configuration, the lean combustion evolves closer to TDC than it could happen for the standard ignition system, with a positive effect on the combustion efficiency. As shown in Table 3, at a fixed lambda value slight decrease in IMEP for the turbulent ignition system configurations was observed for 2000 rpm with gasoline and methane PFI. For methane, at 4000 rpm, the benefits of the turbulent ignition system combustion exceed the disadvantages of the reduction in compression ratio, and in the stoichiometric condition, the operating points show similar IMEP. In lean conditions, the turbulent ignition system strongly improves the combustion stability, as demonstrated by the value of CoV of IMEP (1.9), lower than the commonly accepted threshold (3% [30]). This causes an increase in IMEP. Moreover, despite the lower compression ratio with the pre-chamber, the in-cylinder pressure is higher than that of the traditional spark plug at both stoichiometric and lean modes.

With standard ignition configuration and gasoline, it is possible to reach stable conditions with lambda 1.3. Using methane and standard ignition systems, stable combustion of leaner mixtures cannot be achieved. The use of pre-chamber allows for overcoming this limitation allowing to reach the combustion of lean methane mixtures.

3.1.3. Optical Data Analysis

Optical diagnostics were used to understand the effects of the pre-chamber on the combustion process. High temporal resolution imaging was performed for all selected engine operating conditions. Figures 7 and 8 show the cycle-resolved evolution of the combustion process under stoichiometric and lean conditions at 4000 rpm for both architectures when methane was injected in PFI mode and in the pre-chamber (conditions from 11 to 14). Images were taken from the spark timing and the start of combustion until the flame front reached the optical boundary (3 mm on the radius smaller than the cylinder wall). For brevity, only the results at 4000 rpm were shown.

In the standard configuration, the first luminosity is due to the spark ignition and is indicated by a strong brightness near the spark plug. The flame kernel continues to move in a circular way from this point until it reaches the optical boundary of the combustion chamber. It can be seen that the flame propagates faster in the stoichiometric SI case than in the lean SI case. This result is in good agreement with the scientific literature [9]. In standard combustion, the images show that flame growth is asymmetric, and the shape of the flame deviates from a “circle”. This behavior is even more pronounced in lean combustion, where the flame develops slowly, and its propagation is strongly influenced by the flow dynamics in the chamber and undergoes a greater distortion.

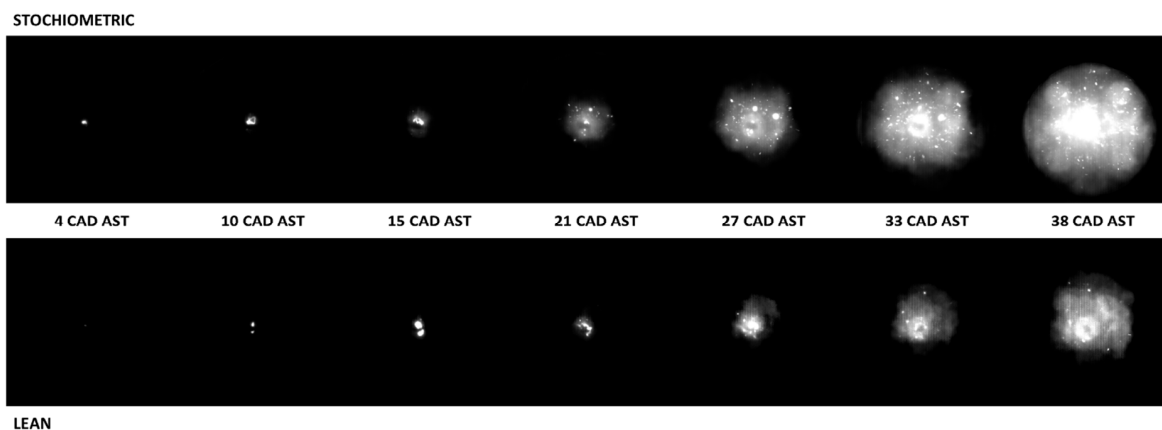


Figure 7. Cycle-resolved 2D measurements of natural luminosity detected at selected crank angles for the conventional spark ignition system under stoichiometric and lean conditions at 4000 rpm. (tests #11–#12).

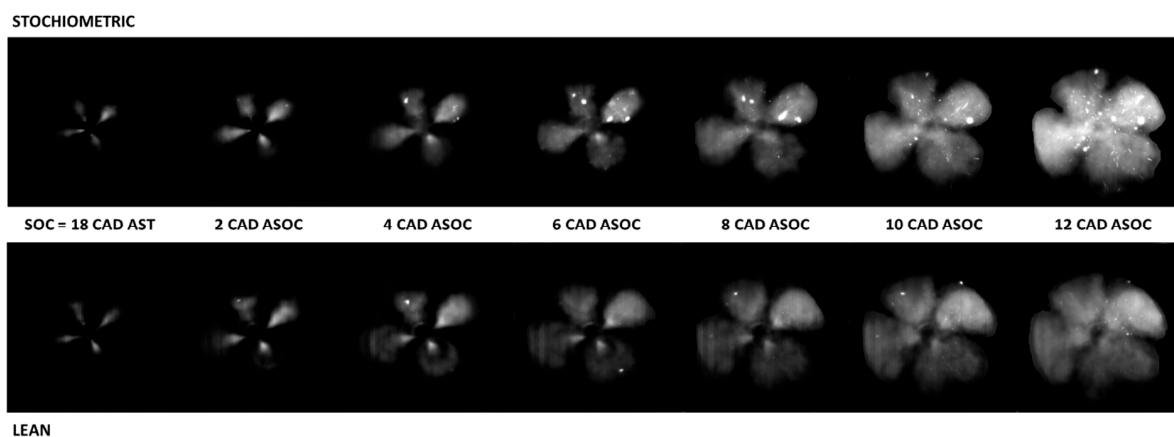


Figure 8. Cycle-resolved 2D measurements of natural luminosity detected at selected crank angles for the pre-chamber ignition system under stoichiometric and lean conditions at 4000 rpm. (tests #13–#14).

A different behavior is observed for the turbulent ignition system (pre-chamber), both in stoichiometric and lean conditions, as shown in Figure 8.

In the turbulent jet ignition configuration, no evidence of spark luminosity was observed due to the pre-chamber geometry. The first evidence of flame is a slight luminosity, indicating the presence of four flames propagating from the pre-chamber with a jet behavior: This $^{\circ}\text{CA}$ has been defined as the “start of combustion” (SOC). The four jets are due to the combustion started in the pre-chamber: A mixture of radicals and products of partial combustion spreads in the main chamber through the small holes in the head of the pre-chamber with a velocity close to 100 m/s. These flames reach the wall and increase their intensity, spreading throughout the volume, changing shape, and resembling a quatrefoil. They show a luminous, dense core in the center of the flame jet.

These four flames are much brighter than the standard flame front and spread to the cylinder wall in fewer crank angle degrees than the standard configuration. The combustion duration is significantly shortened due to the high ignition energy—the energy used to initiate the combustion process—which results in combustion characterized by a lower CoV_{IMEP} compared to the standard ignition, and furthermore, an even leaner mixture can be burned, as shown in Table 3.

In high-time resolution imaging, the contribution of luminosity in the UV, mainly due to the OH^* , is very small and undetectable because the CMOS camera used for this activity has its maximum sensitivity between 380 and 700 nm. To assess whether the contribution of OH^* affects the rate of flame propagation, the evolution of the combustion process was recorded with an acquired UV-visible ICCD camera.

Figure 9 shows the results at 2000 rpm for the standard ignition configuration and pre-chamber.

Figure 9a shows combustion in the stoichiometric condition for the standard configuration when gasoline was injected in the PFI mode (test #1). Evidence of spark ignition is shown by a luminous arc; the flame kernel is easily seen, although its luminosity is much less than that of the spark. The flame kernel has a circular shape and moves radially from the spark plug toward the cylinder wall. The intensity of the chemiluminescent emission is almost uniform within the cloud.

Figure 9b,c show the combustion process at stoichiometric and lean conditions, respectively, for pre-chamber ignition (tests #3 and #5). Gasoline was injected in the PFI mode, and methane was injected in the pre-chamber. Both combustions show four flames propagating out of the pre-chamber with a jet-like behavior igniting the mixture of fresh air and gasoline in the main chamber. The images make it possible to see the start of injection and follow the flame development in the cylinder. These four flames are much brighter

than the normal flame front; they spread very quickly in both stoichiometric and lean conditions and occupy the entire optically accessible area in a few images.

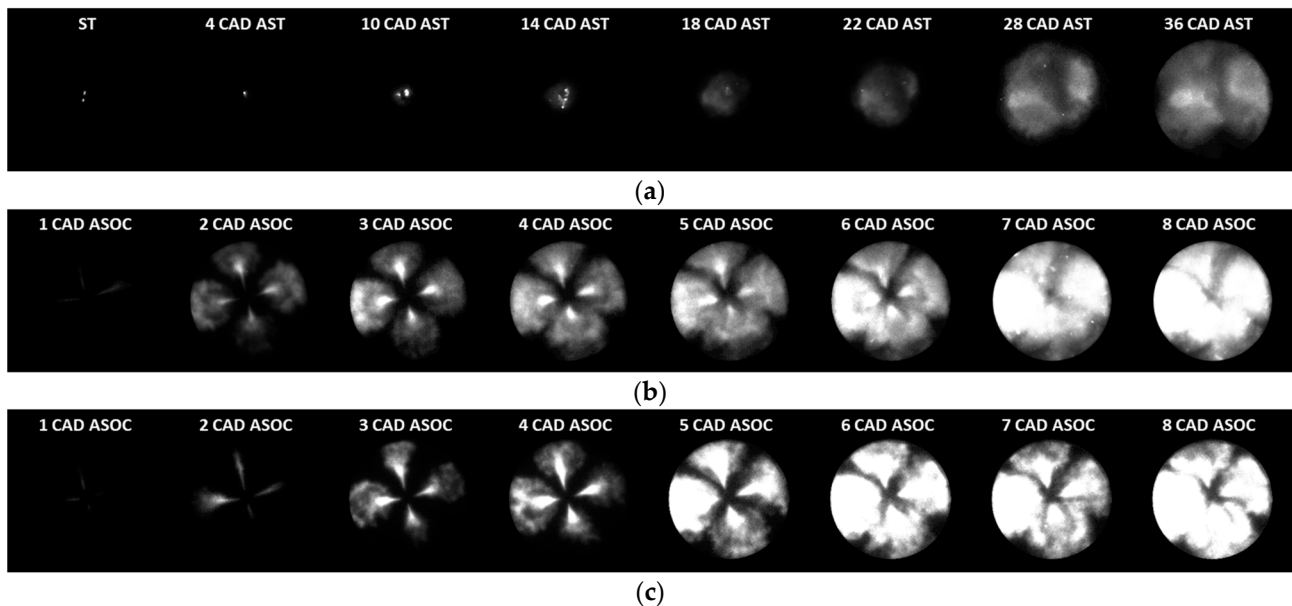


Figure 9. 2D chemiluminescence at 2000 rpm for (a) standard ignition in stoichiometric condition (test #1-gasoline in PFI mode); (b) pre-chamber ignition in stoichiometric condition (test #3-gasoline in PFI mode + methane in the pre-chamber); (c) pre-chamber ignition in lean condition (test #5, gasoline in PFI mode + methane in the pre-chamber, $\lambda = 1.3$).

Figure 10 shows the 2D OH* radical chemiluminescence distribution for the standard ignition configuration and for the pre-chamber at 2000 rpm in the stoichiometric condition. For the standard configuration (Figure 10a), the gasoline was injected into the intake manifold; for the pre-chamber configuration, the methane was injected into the pre-chamber, and the gasoline was injected into the intake manifold (Figure 10b). OH* radical was detected by coupling the ICCD camera with a bandpass filter centered at 310 nm; this radical is used as a flame marker and indicates the location of the reaction zone. In Figure 10a, the distribution of OH* radicals begins near the spark plug during standard ignition and moves in a radial direction toward the chamber wall as the crank angle increases. In Figure 10b, the OH* radicals spread along each jet and toward the cylinder wall.

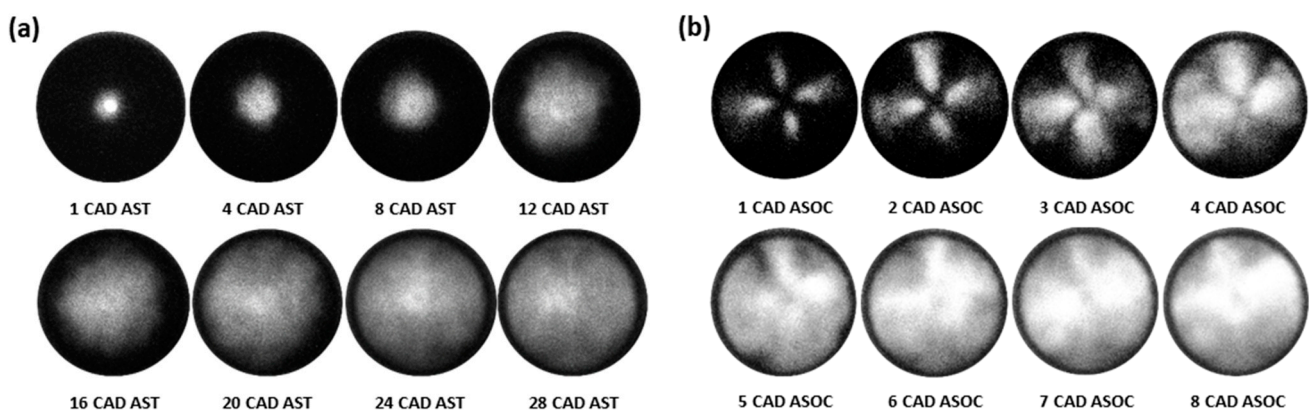


Figure 10. 2D OH* radical chemiluminescence distribution at 310 nm, detected at typical crank angles of the combustion process for the standard (gasoline in PFI mode—test #1—(a)) and pre-chamber (gasoline injected in PFI mode + methane in the pre-chamber—test #3—(b)) ignition at 2000 rpm for stoichiometric condition.

Analysis of the UV-visible signal allows stating that the cycle-resolved visualization can track the combustion process without distortion due to the lack of UV signal detection.

In order to perform a more comprehensive analysis of the impact of ignition configuration and engine operating conditions on the combustion process, the flame radius and flame propagation speed were measured. The following comparison illustrates the calculated flame radius and speed for all the conditions investigated based on the CMOS images. From the previous images, it can be seen that the plasma/flames emerging from the pre-chamber holes reach the boundaries of the viewing window in a couple of °CA due to the high exit velocity, but at this point, the flame has not yet spread throughout the chamber, and there is still unburnt mixture between the adjacent jets. Therefore, the combustion speed cannot be evaluated from the time evolution of the maximum flame radius; otherwise, it would be greatly overestimated. For the same reason, in the case of pre-chamber ignition, the combustion flame speed starts with the first calculated value different from zero, unlike the case of standard ignition. The plasma/flames in the pre-chamber ignition case leave the pre-chamber holes with a velocity much higher than zero, while in the standard ignition case, the flame radius and the flame speed are zero at the start of the spark.

Figure 11a shows the evolution of the flame radius in the standard and pre-chamber at 2000 rpm when methane and gasoline are used. In the pre-chamber, the flame reaches the optical boundary and, thus, the combustion chamber wall much earlier than in the standard combustion under all conditions. In addition, for both configurations, the rise of the flame radius curve is slower at higher lambda values, but this effect is less pronounced for combustion with the pre-chamber compared to standard combustion.

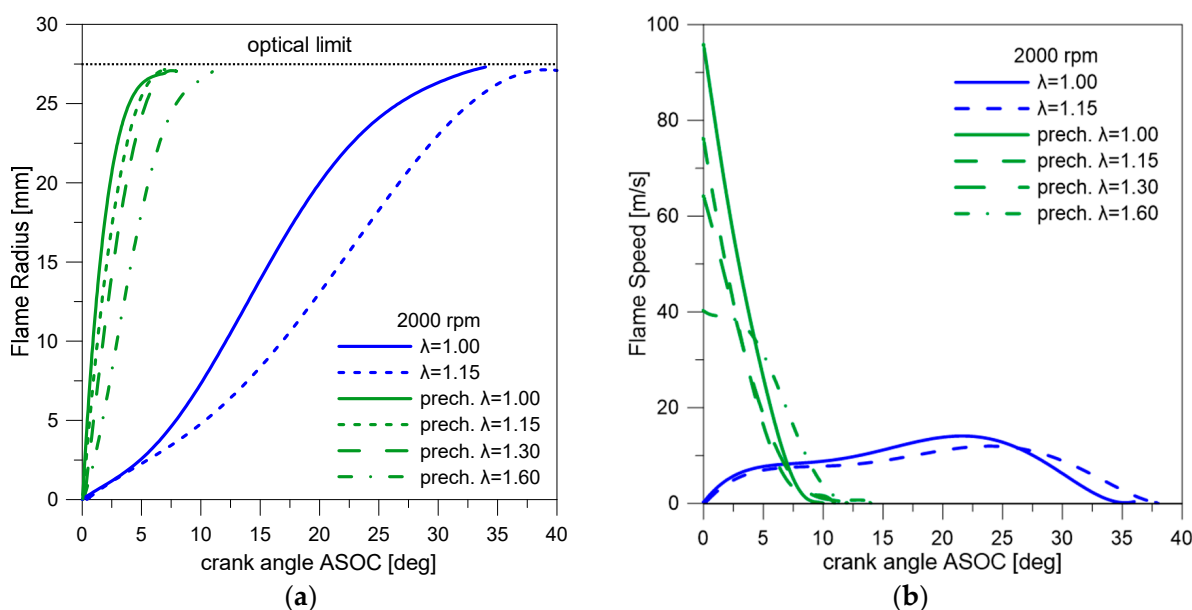


Figure 11. Flame radius (a) and flame front speed (b) evolution for the standard (gasoline in PFI mode) and pre-chamber (gasoline injected in PFI mode + methane in the pre-chamber) configurations at 2000 rpm in lean burn and stoichiometric operations. (tests #1–#6).

For the standard configuration, as seen in Figure 11b, the flame propagation speed shows similar behavior for both lambda values: it increases, reaches a maximum, and then decreases. The peak of the flame speed corresponds to °CA when the flame boundaries start to locally exceed the optically accessible region. After the peak, the decrease in flame speed is due to the growth of the flame area outside the piston window and has only limited quantitative significance [9].

In turbulent jets ignition, the combustion process begins in the pre-chamber, and when the plasma jets enter the cylinder (through the orifices of the pre-chamber), they have remarkable turbulence and speed. Moreover, they are highly reactive due to the presence

of active radicals. This means that the speed of the flame achieved by visualization starts with a high value and then decreases. Compared to the standard spark plug, the maximum value is higher and more advanced in both stoichiometric and lean conditions.

For the standard ignition case, the flame front propagation speed shows similar behavior for both lambda values and engine speeds; it rises, reaches a maximum, and then it decreases, as in tests #1 and #2. Instead, for a turbulent ignition system, the flame front spreads faster from the pre-chamber hole with its maximum speed, so the flame radius starts with the maximum slope without the first flex present in the flame radius of the standard ignition system. However, the rate of increase as well as the time to reach the optical limit, are strongly related to the ignition type and the operating conditions.

In a turbulent ignition system, the flame speed is higher than in the standard spark plug and shows higher and more advanced maximum values in both stoichiometric and lean conditions. Interestingly, advanced and accelerated combustion is not influenced by engine speed. This is attributed to the turbulence generated by the plasma jet from the pre-chamber, which overrides the effects of turbulence caused by engine speed. Figures 12 and 13 show that in the case of the turbulent ignition system, the flame front reaches the optical limit wall at almost identical times for both engine speeds. In addition, the flame velocities are similar, as evidenced by the fact that the flame at 4000 rpm requires twice as many crank angle degrees ($^{\circ}\text{CA}$) to travel the same distance as at 2000 rpm. On the other hand, in the standard configuration at higher engine speed, the combustion speed increases, and the time taken by the front flame to reach the optical limit wall at 4000 rpm is almost half compared to the condition at 2000 rpm.

The turbulent ignition system exhibits faster flame front propagation, resulting in a lower CoV of IMEP compared to the standard spark plug configuration under all conditions. In the case of standard ignition, when the mixture is leaned, the flame front propagation is slowed down due to the reduced flammability of methane in lean conditions. Interestingly, for the turbulent ignition system configuration, the flame propagation is only slightly affected in lean conditions, although it approaches the minimum flammability limit. This observation is noteworthy, considering that the turbulent ignition system keeps flame spread relatively stable even under lean conditions.

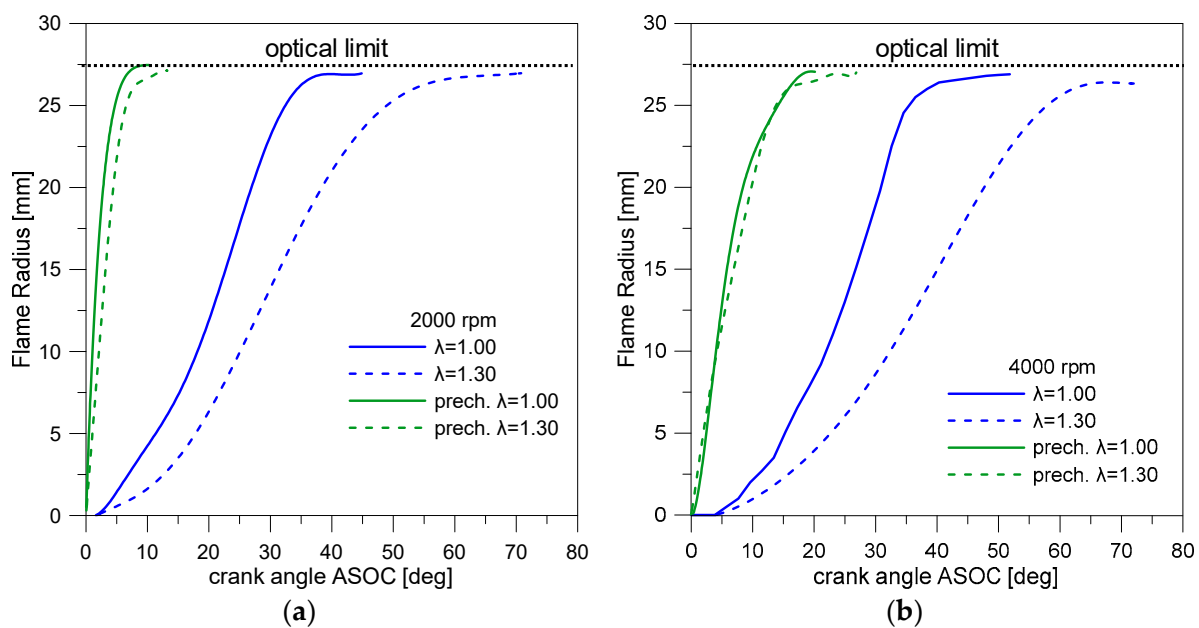


Figure 12. Flame radius evolution with standard and pre-chamber ignition at 2000 rpm (a) and 4000 rpm (b) in lean burn and stoichiometric operations (methane injected in PFI mode + methane in the pre-chamber—tests #7–#14).

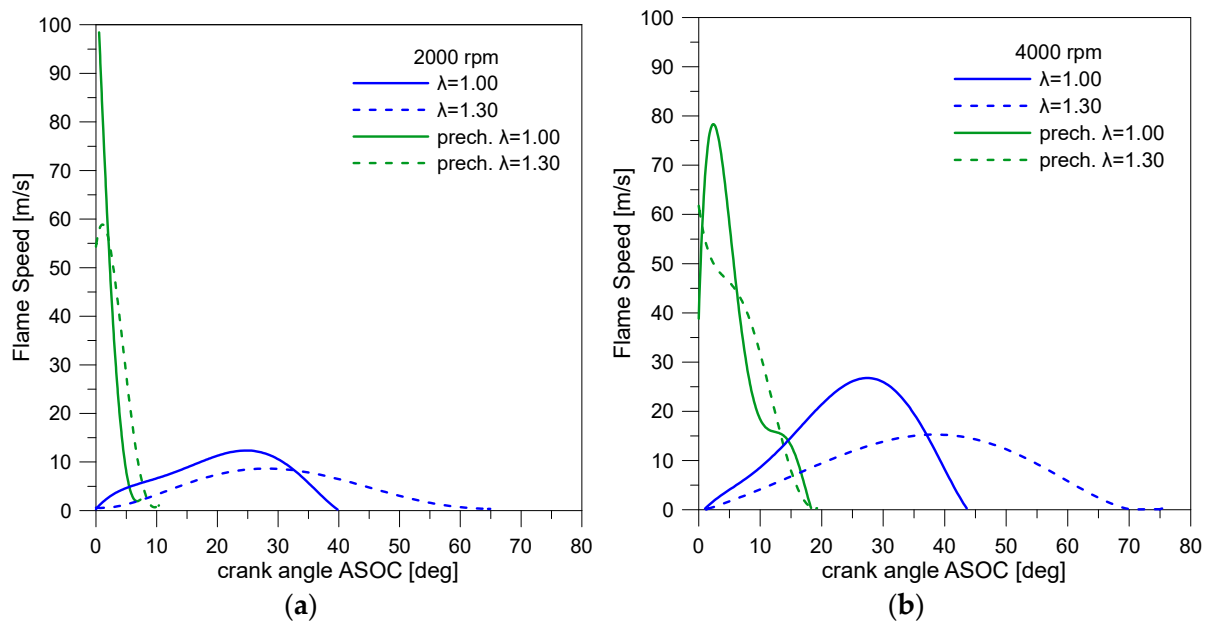


Figure 13. Flame speed with standard and pre-chamber ignition at 2000 rpm (a) and 4000 rpm (b) in lean burn and stoichiometric operations (methane injected in PFI mode + methane in the pre-chamber—tests #7–#14).

3.1.4. Influence of the Conditions in the Cylinder on the Behavior of the Plasma Jet

To investigate the effect of conditions in the cylinder on the characteristics of the plasma jets, the flame speed of each jet was calculated and plotted against the crank angle. This analysis was performed for three different lambda values while injecting methane into the pre-chamber and gasoline into the intake manifold.

Figure 14 on the left shows an image of the combustion chamber captured by a 45° mirror mounted in the elongated piston. The intake valves (I.v.) and exhaust valves (E.v.) are highlighted, as well as the position of the pressure transducer and spark plug/pre-chamber. On the right side of Figure 14, the locations of the plasma jets, strategically selected for analysis, are indicated within the combustion chamber. Each plasma jet was assigned a specific number for identification purposes.

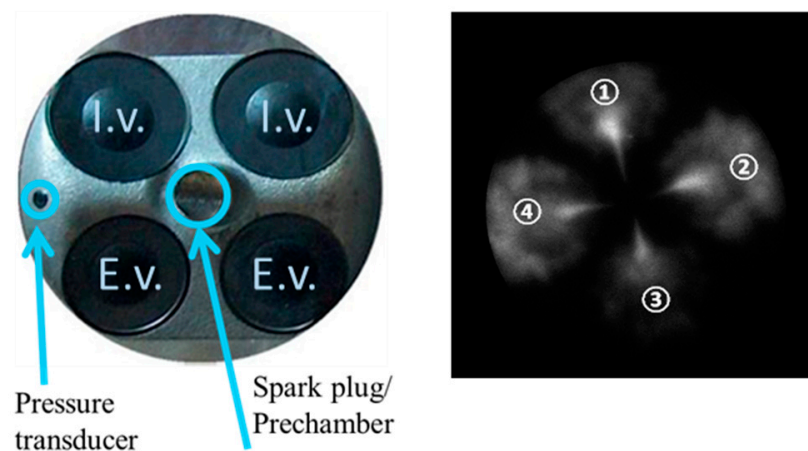


Figure 14. Combustion chamber and analyzed plasma jet positions for flame speed calculation, the symbols ①②③④ in the right side identify the jets for further discussion.

The objective of this section is to investigate how the behavior of each plasma jet is affected by the fuel concentration in the main chamber, represented by the lambda value. Figure 15 shows the flame speeds of the individual plasma jets plotted against crank angle for various lambda values. In addition, the dashed black lines depict the corresponding average flame speed curves. As the lambda values increase, the flame speed curves progressively deviate further away from the average curves.

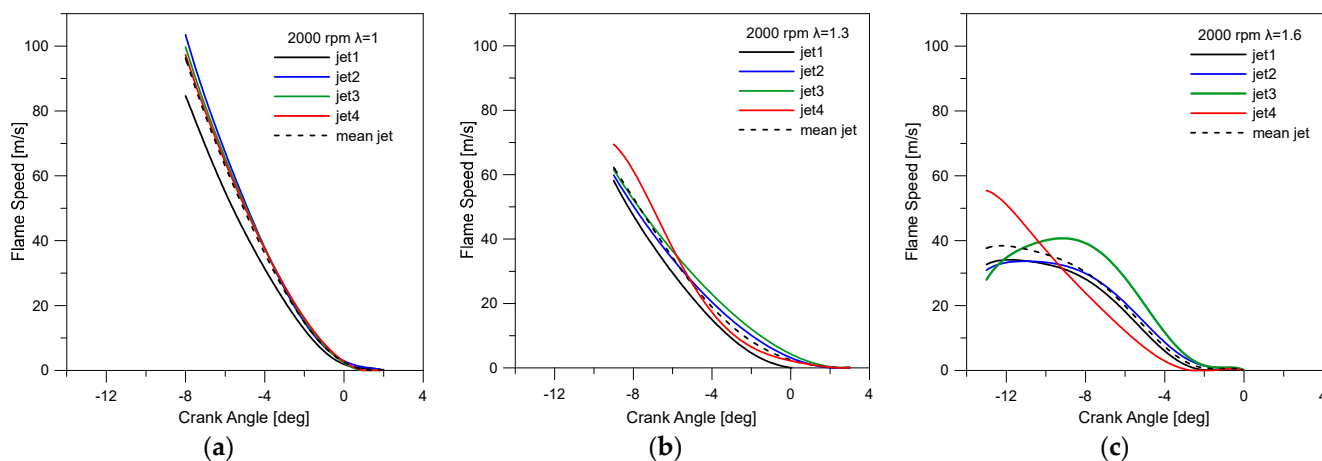


Figure 15. Flame speed of each plasma jet at lambda = 1 (test 3) (a), lambda = 1.3 (test 5) (b), lambda = 1.6 (test 6) (c).

In Figure 15a, when lambda is equal to one, the flame speed curves of each plasma jet are closely aligned with the average flame speed curve. However, as the lambda values increase (Figure 15b,c), the flame speed curves increasingly deviate from the average curves. This indicates that at higher lambda values, the behavior of each plasma jet becomes increasingly different from the others. The probable reason for this is that in lean conditions, the flame speed is low, and flame propagation is more influenced by the fluid dynamic of the combustion chamber. Since the four jets are located at positions characterized by different flow fields, their distortion is different.

3.2. Pre-Chamber in the Commercial SI Engine

3.2.1. Engine Operating Conditions of Real SI Engine

The commercial engine, like the optical one, was tested in two configurations: Standard ignition and pre-chamber.

The tests were conducted at engine speeds of 2000, 3000, 4000, and 5000 rpm using gasoline as fuel. In order to obtain the same cylinder peak pressure in the motored condition in the two configurations, a WOT condition was used for the pre-chamber, and for the standard ignition configuration, the tests were performed at part load (PL). The intake air temperature was set at 298 K, and the cooling water temperature was maintained at 363 K by an AVL water conditioning unit.

For each engine operating condition, the spark timing (ST) was selected to minimize the CoV of the IMEP and achieve maximum brake torque. The injection duration (DOI) was selected to achieve the stoichiometric equivalence ratio and the leanest possible combustion with a reasonable CoV of IMEP (less than 4%). For this reason, the DOI varied depending on the engine point and configuration. For both ignition configurations, the end of fuel injection into the manifold (EOI) was set at 230 °CA BTDC. Table 4 lists all engine parameters and performance at each selected operating condition.

Table 4. Commercial engine parameters and performance at the selected operating conditions.

Configuration	λ	Throttle Valve	Speed [rpm]	ST [° CA BTDC]	DOI [μ s]	IMEP [bar]	CoV _{IMEP} [%]
Standard	1.0	PL	2000	22	4100	7.19	0.82
Standard	1.4	PL	2000	32	3000	5.59	3.67
Pre-chamber	1.0	WOT	2000	17	4400	8.35	0.71
Pre-chamber	1.4	WOT	2000	27	3250	6.49	2.76
Standard	1.0	PL	3000	28	4650	8.11	1.03
Standard	1.3	PL	3000	37	3700	6.80	2.19
Pre-chamber	1.0	WOT	3000	20	4600	9.07	0.66
Pre-chamber	1.3	WOT	3000	41	3500	7.25	2.10
Standard	1.0	PL	4000	27	5000	8.79	1.87
Standard	1.2	PL	4000	32	4200	7.87	2.90
Pre-chamber	1.0	WOT	4000	35	4850	9.65	0.76
Pre-chamber	1.2	WOT	4000	47	4100	8.63	2.60
Standard	1.0	PL	5000	25	5000	9.24	2.63
Standard	1.1	PL	5000	27	4600	8.81	2.80
Pre-chamber	1.0	WOT	5000	48	5000	9.63	1.86
Pre-chamber	1.1	WOT	5000	40	4450	8.62	2.80

3.2.2. Indicated Data Analysis

To compare combustion with the turbulent ignition system to standard ignition, in-cylinder pressures and ROHR for all engine speeds, lambda values, and configurations are shown in Figure 16.

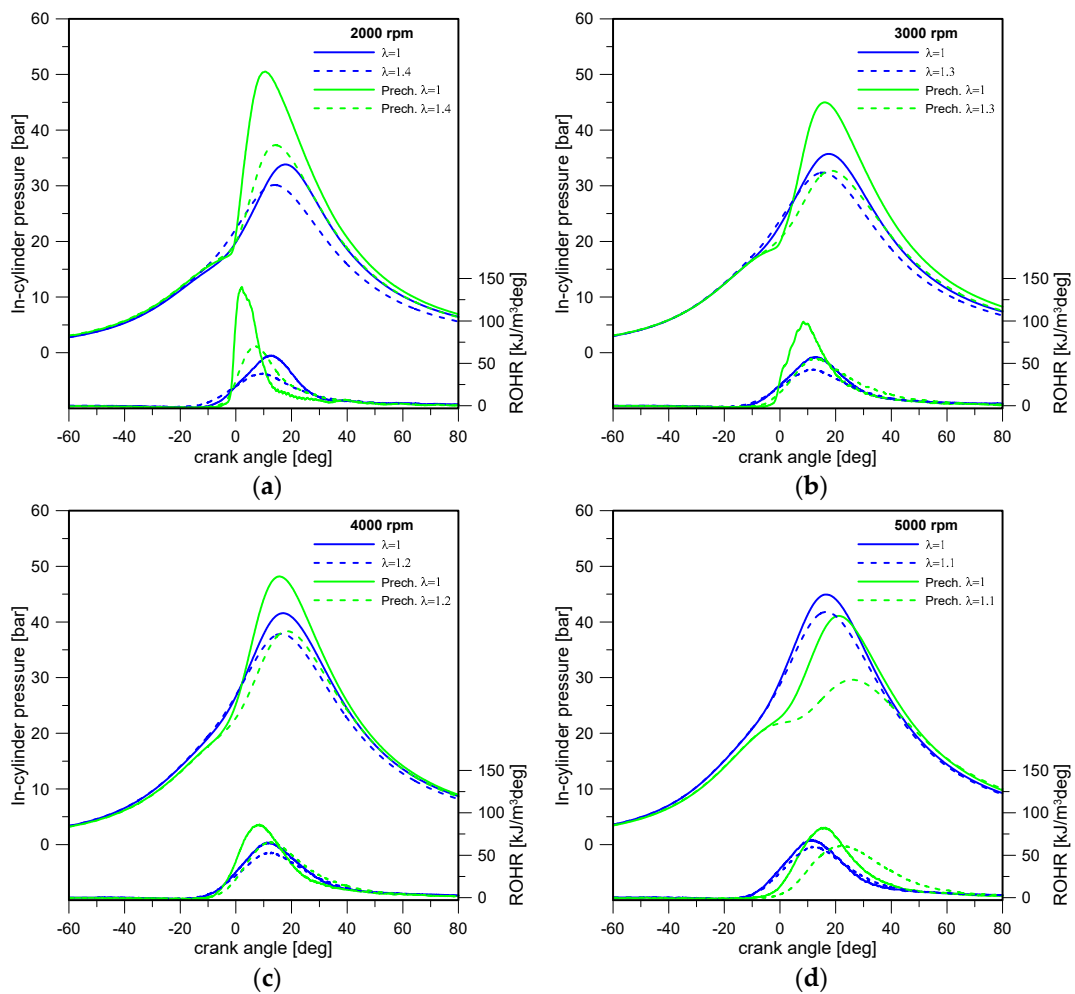


Figure 16. In-cylinder pressure and ROHR curves for pre-chamber and standard ignition system under stoichiometric and lean conditions at 2000 (a), 3000 (b), 4000 (c), and 5000 (d) rpm.

In standard ignition, the part-load condition was used to compensate for the reduction in compression ratio caused by the pre-chamber. To achieve the same compression ratio, the motored pressure was equalized for both configurations.

With the pre-chamber configuration, the maximum pressure in the cylinder is higher than with the conventional spark plug under all conditions, despite the lower compression ratio. This is due to a combination of two factors: First, the partial load conditions for the conventional spark, and second, the faster combustion in the pre-chamber and, thus, a better combustion phasing.

In particular, at $\lambda = 1$ the ROHR shows a narrow and highest peak, which is probably due to the early onset of ignition, and a slightly larger peak at $\lambda = 1.4$. This is due to faster combustion related to the faster propagation of the flame front, typical of turbulent ignition systems [31]. The faster propagation leads to a deeper penetration of the flame in the main combustion chamber and, thus, to significantly faster combustion in the main chamber.

At 2000 rpm, for both stoichiometric and lean modes, the quantity of energy available in the combustion chamber is similar but slightly higher for the turbulent ignition system due to the air partialization of the standard spark plug configuration; instead, the engine efficiency, evaluated as ISFC showed in Figure 17, is much higher in the turbulent ignition system than in the standard ignition. On the other hand, at the other engine speeds, both at stoichiometric and lean values, the amount of fuel injected into the combustion chamber is slightly higher for the standard ignition configuration, and yet the IMEP and efficiency are always higher with the turbulent ignition system. In all configurations, the fuel was injected at the same time and with the same pressure; there are no differences in the mixture formation, and therefore, in the lambda distribution in the combustion chamber at ST and during flame front propagation, the main difference is observed in the flame front propagation due to the turbulence generated by the pre-chamber, as shown by the optical investigation previously reported.

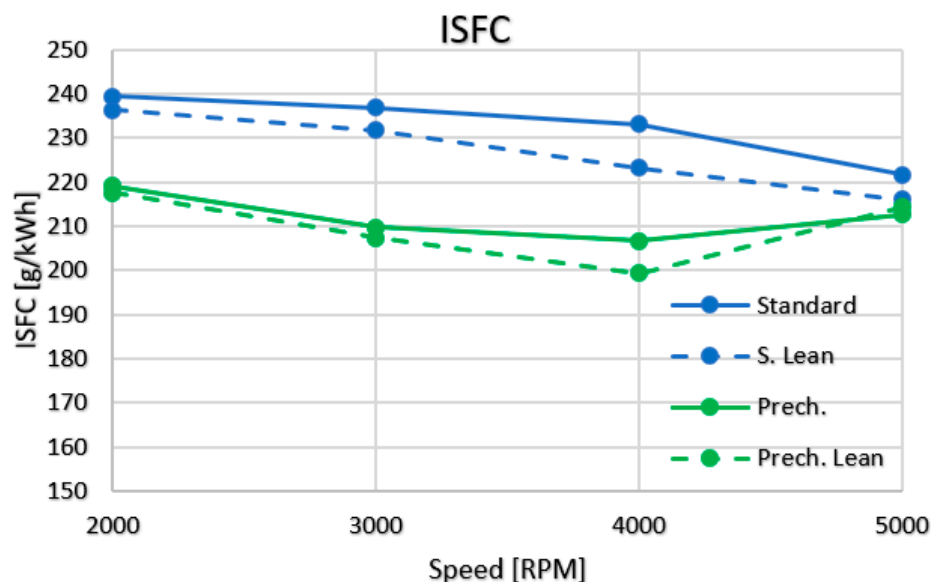


Figure 17. ISFC measured for both ignition types in stoichiometric and lean configurations at 2000, 3000, 4000, and 5000 rpm.

In Figure 16d, the pressure cycles and the ROHR at 5000 rpm are reported. For the standard ignition configuration (PL), the combustion is faster and more advanced in the stoichiometric case, as evidenced by the ROHR curves. With the turbulent ignition system (WOT), the combustion acceleration results in a higher peak of the ROHR, which has a greater slope than the standard ignition. Moreover, in the lean condition, the combustion evolves closer to the TDC in the standard ignition mode because of the advanced spark timing, as can be seen in Table 4, improving the combustion efficiency and producing

a higher effective pressure. It is worth noting that despite the increase in IMEP, in the lean condition, the efficiency is higher for the turbulent ignition system due to the shorter injection duration compared to the standard ignition one. At 5000 rpm-stoichiometric condition, the turbulent ignition system strongly improves the stability of the combustion and consequently causes the increase in the IMEP (averaged on 500 consecutive cycles). A slight decrease in the IMEP values for the turbulent ignition configuration was observed only at 5000 rpm lean condition may be due to the worst mixture formation into the pre-chamber caused by the lower time available. Table 4 presents the values of IMEP, its corresponding coefficient of variation (CoV), and the lambda for the different conditions studied. Across all conditions, the advantages of the turbulent ignition system combustion outweigh the drawbacks of the reduced compression ratio. The CoV of IMEP serves as an indicator of cyclic variability derived from pressure data, and it should ideally be below 3% to signify a highly stable combustion process [31,32]. The CoV of IMEP is lower for the turbulent ignition system suggesting a more stable combustion: the reduction in CoV can be ascribed to the increased turbulent flame speed rather than the laminar flame speed, which depends on the lambda value. Instead, at 5000 rpm-lean conditions, the CoV of IMEP is higher for the turbulent ignition system, probably because at higher engine speeds, the pre-chamber scavenging and subsequent filling are worsened. This could determine a much more difficult and unstable ignition.

The effect of ignition strategy and lambda value on combustion is also well described by the indicated specific fuel consumption (ISFC). In Figure 17, it can be seen that the ISFC in the lean condition is lower for both ignition modes, as expected. For pre-chamber, the ISFC is much lower than for standard ignition, except at 5000 rpm, where pre-chamber scavenging and mixture formation need to be improved.

3.2.3. Exhaust Gas Emissions

Figure 18 shows CO, CO₂, HC, and NO_x emissions in g/kWh at different engine speeds and lambda values. Both CO and CO₂ concentrations are lower in the turbulent ignition configuration than in the standard ignition configuration, despite the larger fuel quantity at some of the tested conditions. This indicates more efficient combustion in the pre-chamber configuration compared to the standard ignition. The only exception is CO at high rpm (Figure 18d), where the efficiency of the turbulent ignition system decreases: This is confirmed by the indicated data analysis at 5000 rpm described above.

The more efficient combustion is also evident in the turbulent ignition configuration, considering the lower HC concentrations, probably due to faster and more advanced combustion, leading to a higher temperature in the cylinder, which promotes fuel evaporation. Another factor to take into account is the reduced quenching distance resulting from accelerated combustion and the subsequent decrease in thermal dispersion. NO_x emissions, which are highly dependent on the in-cylinder temperature, are particularly affected by these changes. In absolute terms, the turbulent ignition configuration results in higher NO_x emissions due to faster and more advanced combustion, leading to higher cylinder temperatures. However, if they are expressed in g/kWh, they are affected by the lower fuel consumption measured with pre-chamber combustion so that their value is comparable and lower than for the standard ignition configuration, except under stoichiometric conditions.

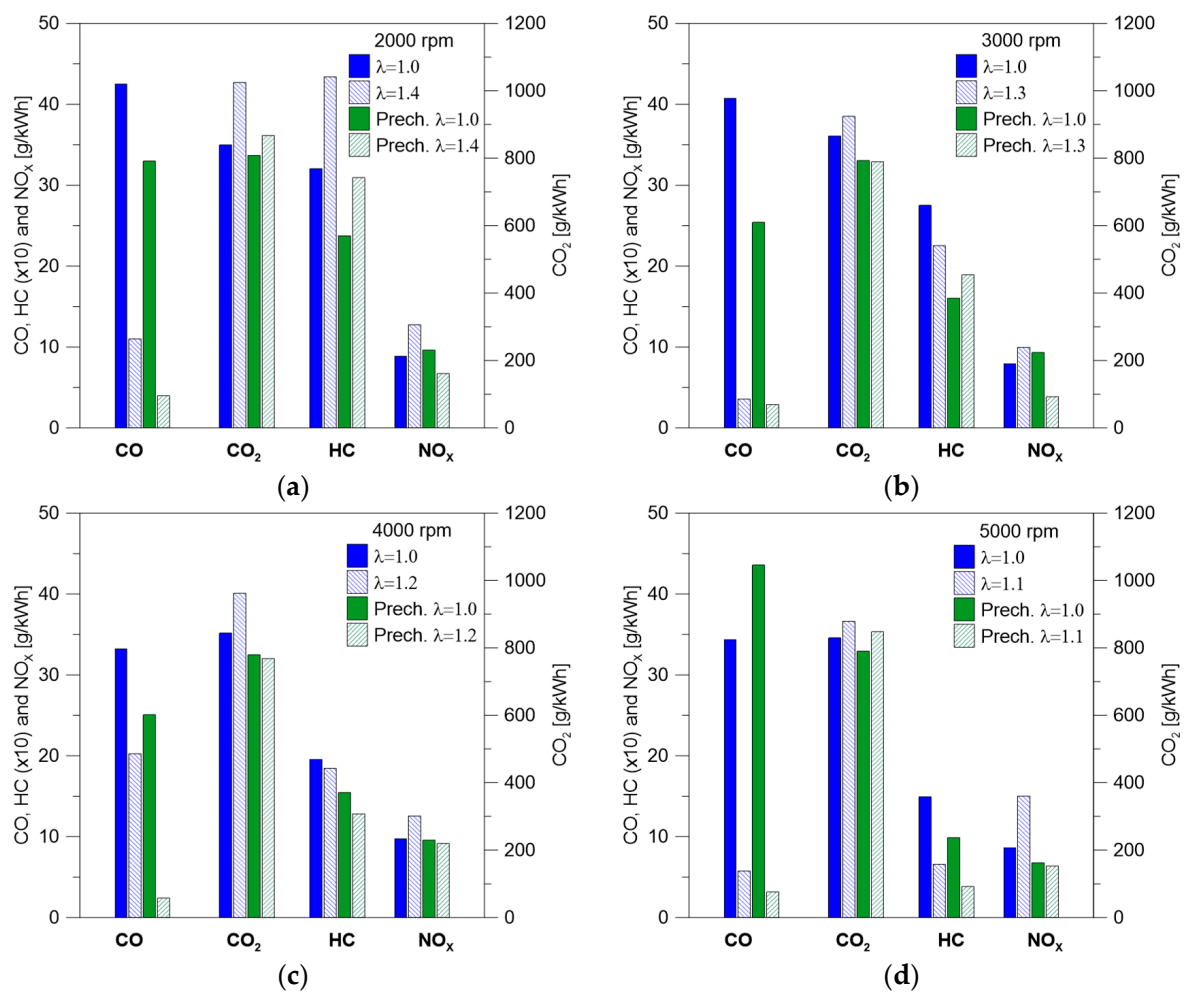


Figure 18. CO, CO₂, HC, and NO_x emissions for all the tested conditions at 2000 (a), 3000 (b), 4000 (c), and 5000 (d) rpm.

4. Conclusions

The aim of this paper is to investigate the effect on engine stability and efficiency in stoichiometric and lean-burn operation conditions of a turbulent ignition system suitably designed for a small spark ignition engine. The pre-chamber was designed to be integrated into the original engine head, particularly at the unmodified location of the spark plug, and it is equipped with both a commercial spark plug and an injector, being used in both active and passive modes.

Optical diagnostics revealed that the turbulent ignition system had faster and more advanced combustion compared to the standard ignition system, regardless of engine speed. It overcame lean mixture limitations maintaining flame propagation even near minimum flammability limits. The pre-chamber improved the lean operating limit for methane fueling, ensuring stable operation at high excess air. In addition, experiments on a commercial engine with a passive pre-chamber showed higher in-cylinder pressure and lower CoV of IMEP, indicating improved combustion stability except at the highest engine speed. The turbulent ignition system demonstrated lower ISFC and lower specific exhaust emissions, indicating more efficient combustion, except at 5000 rpm, where pre-chamber optimization is required due to suboptimal scavenging and mixture formation. Overall, the turbulent ignition system provided more energy for combustion initiation and faster flame propagation, which improved lean mixture combustion and overall engine efficiency. The main advantage of the system is that it extends the flammability limit of the air-fuel mixture, ensuring consistent, high-quality combustion.

Author Contributions: Conceptualization, P.S. and B.M.V.; methodology, P.S. and F.C.; software, F.C.; formal analysis, C.T.; investigation, P.S., F.C. and S.D.I.; resources, B.M.V.; data curation, C.T.; writing—original draft preparation, P.S., C.T. and S.D.I.; writing—review and editing, C.T. and F.C.; supervision, P.S.; funding acquisition, B.M.V. All authors have read and agreed to the published version of the manuscript.

Funding: This research received no external funding.

Data Availability Statement: The data presented in this study are available on request from the corresponding author.

Acknowledgments: The authors are grateful to Carlo Rossi and Bruno Sgammato for the assessment of the optical engine and for their support in the experimental activities.

Conflicts of Interest: The authors declare no conflict of interest.

Abbreviations

°CA	Crank Angle degree
BTDC	Before Top Dead Center
CCV	Cycle-to-Cycle Variation
CMOS	Complementary Metal-Oxide Semiconductor
CO	Carbon Monoxide
CoV	Coefficient of Variation
DOI	Duration of injection
ETU	Engine Timing Unit
GDI	Gasoline Direct Injection
HC	Hydrocarbons
ICCD	Intensified Charge Coupled Device
IMEP	Indicated Mean Effective Pressure
ISFC	Indicated Specific Fuel Consumption
PC	Pre-Chamber
PFI	Port Fuel Injection
PL	Partial Load
ROHR	Rate of Heat Release
rpm	rotation per minute
SI	Spark Ignition
SIS	Standard Ignition System
SOC	Start of Combustion
ST	Spark Timing
TDC	Top Dead Center
TTL	Transistor-Transistor Logic
WOT	Wide Open Throttle

References

1. Najjar, Y.S.H. Comparison of performance of a greener direct-injection stratified-charge (DISC) engine with a spark-ignition engine using a simplified model. *Energy* **2011**, *36*, 4136–4143. [[CrossRef](#)]
2. Zhao, F.; Lai, M.C.; Harrington, D.L. Automotive spark-ignited direct-injection gasoline engine. *Prog. Energy Combust. Sci.* **1999**, *25*, 437–562. [[CrossRef](#)]
3. Zhao, F.; Lai, M.C.; Harrington, D.L. *The Spray Characteristics of Automotive Port Fuel Injection—A Critical Review*; SAE Technical Paper No. 950506; SAE International: Warrendale, PA, USA, 2015.
4. Harada, J.; Tomita, T.; Mizuno, H.; Mashiki Ito, Y. *Development of a Direct Injection Gasoline Engine*; SAE Technical Paper No. 974054; SAE International: Warrendale, PA, USA, 1997.
5. Zhao, F.; Lai, M.C.; Harrington, D.L. *A Review of Mixture Preparation and Combustion Control Strategies for Spark-Ignited Direct-Injection Gasoline Engine*; SAE Technical Paper No. 970627; SAE International: Warrendale, PA, USA, 1997.
6. Ando, H.; Arcoumanis, C. Mixture preparation and combustion in four-stroke direct-injection gasoline engines. In *Flow Combust. Reciprocating Engines*; Springer: Berlin/Heidelberg, Germany, 2009; pp. 137–171.

7. Sementa, P.; Catapano, F.; Di Iorio, S.; Todino, M.; Vaglieco, B.M. *Analysis of the Combustion Process of SI Engines Equipped with Non-Conventional Ignition System Architecture*; SAE Technical Paper No. 2020-37-0035; SAE International: Warrendale, PA, USA, 2020.
8. Cathcart, G.; Tubb, J. *Application of Air Assisted Direct Fuel Injection to Pressure Charged Gasoline Engines*; SAE Technical Paper No. 2002-01-0705; SAE International: Warrendale, PA, USA, 2002.
9. Tornatore, C.; Sjöberg, M. Optical Investigation of a Partial Fuel Stratification Strategy to Stabilize Overall Lean Operation of a DISI Engine Fueled with Gasoline and E30. *Energies* **2021**, *14*, 396. [[CrossRef](#)]
10. Qian, Y.; Li, Z.; Yu, L.; Wang, X.; Lu, X. Review of the state-of-the-art of particulate matter emissions from modern gasoline fueled engines. *Appl. Energy* **2019**, *238*, 1269–1298. [[CrossRef](#)]
11. Zigan, L.; Schmitz, I.; Flugel, A.; Wensing, M.; Leipertz, A. Structure of evaporating single- and multicomponent fuel spray for 2nd generation gasoline direct injection. *Fuel* **2011**, *90*, 348–363. [[CrossRef](#)]
12. Maricq, M.M.; Szente, J.J.; Jahr, K. The impact of ethanol fuel blends on PM emissions from a light-duty GDI vehicle. *Aerosol Sci. Technol.* **2012**, *46*, 576–583. [[CrossRef](#)]
13. Myung, C.L.; Kim, J.; Choi, K.; Hwang, I.G.; Park, S. Comparative study of engine control strategies for particulate emissions from direct injection light-duty vehicle fueled with gasoline and liquid phase liquefied petroleum gas (LPG). *Fuel* **2012**, *94*, 348–355. [[CrossRef](#)]
14. Benajes, J.; Novella, R.; Gomez-Soriano, J.; Martinez-Hernandez, P.J.; Dabiri, M. Evaluation of the passive pre-chamber ignition concept for future high compression ratio turbocharged spark-ignition engines. *Appl. Energy* **2019**, *248*, 576–588. [[CrossRef](#)]
15. Boretti, A.; Jin, S.H.; Brear, M.; Zakis, G.; Attard, W.; Watson, H.; Brewster, S.; Bryce, W. Experimental and numerical study of a spark ignition engine with air-assisted direct injection. *Proc. Inst. Mech. Eng. Part D J. Automob. Eng.* **2008**, *222*, 1103–1119. [[CrossRef](#)]
16. Sementa, P.; Catapano, F.; Di Iorio, S.; Todino, M.; Vaglieco, B.M. *Turbulent Jet Ignition Effect on Exhaust Emission and Efficiency of a SI Small Engine Fueled with Methane and Gasoline*; SAE Technical Paper No. 2020-24-0013; SAE International: Warrendale, PA, USA, 2020.
17. Alvarez, C.E.C.; Couto, E.G.; Roso, V.R.; Thiriet, A.B.; Valle, R.M. A review of pre-chamber ignition systems as lean combustion technology for SI engines. *Appl. Therm. Eng.* **2018**, *128*, 107–120. [[CrossRef](#)]
18. Schumacher, M.; Wensing, M. *A Gasoline Fuelled Pre-Chamber Ignition System for homogenous Lean Combustion Processes*; SAE Technical Paper No. 2016-01-2176; SAE International: Warrendale, PA, USA, 2016.
19. Böwing, R. *Der Einfluß von Zündung und Zylinderinnenströmung auf die Verbrennung in Ottomotoren mit Hoher Ladungsverdünnung*. Ph.D. Dissertation, RWTH Aachen, Aachen, Germany, 2000.
20. Lumsden, G.; Watson, H.C. *Optimum Control of an S.I. Engine with a $\lambda = 5$ Capability*; SAE Technical Paper No. 950689; SAE International: Warrendale, PA, USA, 1995.
21. Liu, X.; Echeverri Marquez, M.; Sanal, S.; Silva, M.; AlRamadan, A.S.; Cenker, E.; Sharma, P.; Magnotti, G.; Turner, J.W.G.; Im, H.G. Computational assessment of the effects of pre-chamber and piston geometries on the combustion characteristics of an optical pre-chamber engine. *Fuel* **2023**, *341*, 127659. [[CrossRef](#)]
22. Hua, J.; Zhou, L.; Gao, Q.; Feng, Z.; Wei, H. Influence of pre-chamber structure and injection parameters on engine performance and combustion characteristics in a turbulent jet ignition (TJI) engine. *Fuel* **2021**, *283*, 119236. [[CrossRef](#)]
23. Distaso, E.; Amirante, R.; Cassone, E.; Catapano, F.; De Palma, P.; Sementa, P.; Tamburrano, P. *Experimental and Numerical Analysis of a Pre-Chamber Turbulent Jet Ignition Combustion System*; SAE Technical Paper No. 2019-24-0018; SAE International: Warrendale, PA, USA, 2019.
24. Tang, Q.; Sampath, R.; Marquez, M.E.; Sharma, P.; Hlaing, P.; Ben Houidi, M.; Cenker, E.; Chang, J.; Magnotti, G.; Johansson, B. Optical diagnostics on the pre-chamber jet and main chamber ignition in the active pre-chamber combustion (PCC). *Combust Flame* **2021**, *228*, 218–235. [[CrossRef](#)]
25. Bunce, M.; Blaxill, H.; Kulatilaka, W.; Jiang, N. *The Effects of Turbulent Jet Characteristics on Engine Performance Using a Pre-Chamber Combustor*; SAE Technical Paper No. 2014-01-1195; SAE International: Warrendale, PA, USA, 2014.
26. Gentz, G.; Thelen, B.; Gholamisheeri, M.; Litke, P.; Brown, A.; Hoke, J.; Toulson, E. A study of the influence of orifice diameter on a turbulent jet ignition system through combustion visualization and performance characterization in a rapid compression machine. *Appl. Therm. Eng.* **2015**, *81*, 399–411. [[CrossRef](#)]
27. Wallesten, J.; Chomiak, J. *Investigation of Spark Position Effects in a Small Pre-chamber on Ignition and Early Flame Propagation*; SAE Technical Paper No. 2000-01-2839; SAE International: Warrendale, PA, USA, 2000.
28. Lu, C.; Song, E.; Xu, C.; Ni, Z.; Yang, X.; Dong, Q. Analysis of Performance of Passive Pre-Chamber on a Lean-Burn Natural Gas Engine under Low Load. *J. Mar. Sci. Eng.* **2023**, *11*, 596. [[CrossRef](#)]
29. Antolini, J.; Sementa, P.; Tornatore, C.; Catapano, F.; Vaglieco, B.M.; Desantes, J.M.; López, J.J. Effect of passive pre-chamber orifice diameter on the methane combustion process in an optically accessible SI engine. *Fuel* **2023**, *341*, 126990. [[CrossRef](#)]
30. Karim, G.A. *Dual-Fuel Diesel Engines*, 1st ed.; CRC Press: Boca Raton, FL, USA, 2015.

31. Toulson, E.; Schock, H.; Attard, W. *A Review of Pre-Chamber Initiated Jet Ignition Combustion Systems*; SAE Technical Paper No. 2010-01-2263; SAE International: Warrendale, PA, USA, 2010.
32. Fansler, T.D.; Reuss, D.L.; Sick, V.; Dahms, R.N. Invited Review: Combustion instability in spray-guided stratified-charge engines: A review. *Int. J. Engine Res.* **2015**, *16*, 260–305. [[CrossRef](#)]

Disclaimer/Publisher’s Note: The statements, opinions and data contained in all publications are solely those of the individual author(s) and contributor(s) and not of MDPI and/or the editor(s). MDPI and/or the editor(s) disclaim responsibility for any injury to people or property resulting from any ideas, methods, instructions or products referred to in the content.